A NEW POSTIRRADIATION MECHANICAL BEHAVIOR TEST—THE MINIATURIZED DISK BEND TEST

MICHAEL P. MANAHAN *Battelle, Columbus Laboratories*
505 King Avenue, Columbus, Ohio 43201

Received December 30, 1982
Accepted for Publication May 27, 1983

A Miniaturized Disk Bend Test (MDBT) capable of extracting postirradiation mechanical behavior information from disk-shaped specimens no larger than those used for transmission electron microscopy has been successfully developed. Finite element analysis is performed to convert the experimentally measured data into useful engineering information. A new finite element frictional contact boundary condition model has been developed that is essential in modeling the nonuniform strain fields present in the MDBT specimen. The MDBT methodology has been shown to be capable of delivering uniaxial stress/strain information with approximately the same level of accuracy as that present in the more conventional uniaxial tensile testing approach. A data inversion strategy has been developed and applied to irradiated materials to determine uniaxial tensile behavior. Since neutron irradiation costs scale with specimen volume, this miniaturized mechanical behavior test can now provide significant savings in irradiation testing costs for nuclear materials used in fusion and other nuclear technologies. In addition, it is now possible to provide mechanical behavior information not ordinarily obtainable due to space limitations in irradiation experiments, and thus expedite alloy development investigations.

I. INTRODUCTION

There exist many promising advanced alloy systems for possible fission and fusion reactor applications, and, of course, within each system myriads of thermomechanical treatments and processing conditions can be developed. The mechanical behavior of prime candidates from each of these alloy systems needs to be readily determined in the postirradiated state. To this end, a Miniaturized Disk Bend Test (MDBT), which is capable of determining most of the mechanical behavior information desired to screen many alloy systems in the postirradiated state in a timely and cost-effective fashion, has been developed.

Neutron irradiation space for materials investigations is limited and costly. It is therefore desirable to use specimens of minimum volume. Disk-shaped specimens no larger than those used for transmission electron microscopy (TEM) were chosen. These specimens are 20 to 500 times smaller than the more conventional uniaxial tensile specimens currently being used for postirradiation testing. To graphically depict the size scale involved in the MDBT, an MDBT specimen is compared to the more conventional postirradiation uniaxial tensile specimen in Fig. 1. Since neutron irradiation costs scale with specimen

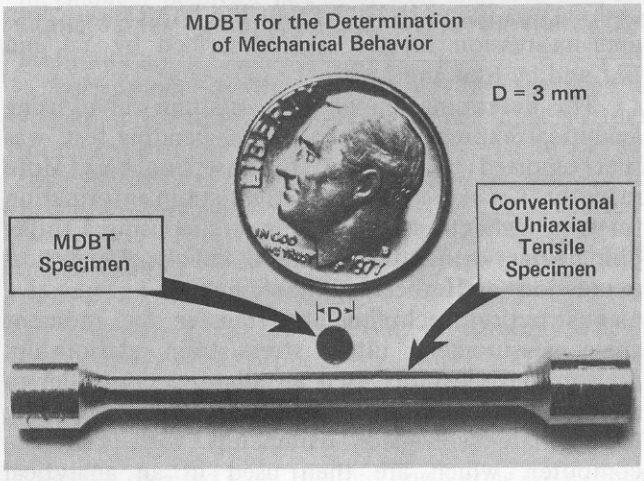

Fig. 1. MDBT specimen compared to conventional postirradiation button end uniaxial tensile specimen.

volume, this miniaturized mechanical behavior test can now provide significant savings in irradiation testing costs for nuclear materials investigations for fission and fusion reactor applications. In addition, it is possible to provide mechanical behavior information not ordinarily obtainable due to space limitations in irradiation experiments, and therefore a substantial time savings in alloy development programs can now be realized. Of course, the MDBT is applicable to materials investigations for other nuclear technologies as well as technologies requiring mechanical behavior characterization from a small volume of material. Also, the MDBT is somewhat unique in that the measurements are made in a stress field that is biaxial, and the data conversion method accounts for multiaxial stress states. Thus, it is readily possible to report biaxial behavior as well as referring back to the more conventional uniaxial behavior. Therefore, the MDBT may also be applicable to technologies desiring biaxial response information. An additional advantage of the MDBT is that the low residual activity of the TEM disks in general would preclude the need for high-activity hot-cell testing techniques, and therefore the radioactive disks can be more easily and quickly handled. Since TEM disk irradiations are standard at most fission reactor irradiation facilities, there are no additional irradiation capsule redesign costs associated with the MDBT methodology.

There are two principal conceptual innovations present in the MDBT. The first innovation is to use bending to extract mechanical behavior information from a very small sample as opposed to the more standard approach of using uniaxial tensile loading requiring gripping extensions. The second innovation is the use of the finite element method to extract useful engineering information from the experimental data. While the former innovation has been suggested and used also by others[1-4] with analytical modeling, the latter was first proposed by Manahan and Argon,[5] and derives its motivation from the impression creep and impression fatigue tests described by Yu and Li,[6] and by Chu and Li.[7,8]

The determination of a stress/strain curve, using analytical expressions from a pure bending test, was first reported by Herbert[1] for cast iron bars. More recently, Crocker[2] obtained stress/strain information for large deflections and plastic strains using a three-point rotary bend test. He used the same analytical expressions as Herbert and implemented a progressive reconstruction technique to transfer the moment angle measurements into a stress/strain relationship. Stelson and Gossard[3] used an adaptive controller to measure force and displacement during brakeforming to estimate workpiece parameters with a microcomputer, which are then used in an analytical elastic-plastic material model to predict correct final punch position. Although these earlier developments have been useful, particularly in the metals-forming industry, they are not readily adaptable to post-irradiation mechanical behavior testing because of large size and awkward loading configuration. For this application, a simply supported miniaturized disk of the size of TEM specimens is advantageous. A similar specimen and loading configuration to provide for ductility screening of samples with very small ductility has also been developed by Huang et al. using small-strain analytical expressions.[4] The advantage of the finite element method for data inversion in the MDBT is that it permits the extraction of both plastic resistance and creep resistance from the raw data in addition to the information on ductility from irradiated samples exhibiting moderate to large levels of strain to fracture and with a minimum of material.

An attempt has been made to design the MDBT from its conception to be capable of determining from biaxial measurements additional information such as stress relaxation behavior, creep response, creep ductility, *S-N* fatigue response, ductile/brittle transition temperature, fracture modes, and fracture stress and strain. Several scoping experiments and analyses indicate that the MDBT technique, with straightforward development, has promising possibilities of delivering this information.[9] The capability of delivering information on fracture modes has already been demonstrated.[9,10] The details of these developments are beyond the scope of this paper and will be presented elsewhere. The primary focus of this paper is the demonstration of the validity of the MDBT methodology for uniaxial tensile testing, estimation of its accuracy, and application to the inversion of postirradiation data.

Section II provides a description of the MDBT experimental design as well as some key preirradiation experimental results. Section III provides a brief discussion of the new finite element friction-gap boundary condition model. Demonstration of the validity of the MDBT methodology and comparison of the accuracy of the MDBT with conventional uniaxial tensile testing are presented in Secs. IV and V. The MDBT strategy for postirradiation mechanical behavior experimental data inversion is presented and applied to some irradiated specimens in Sec. VI. Finally, Sec. VII provides a fundamental interpretation of the experimental central load/deflection curve.

II. PREIRRADIATION EXPERIMENTAL RESULTS

The MDBT experimental configuration consists of a simply supported centrally loaded specimen. The specimen disk, which has nominal dimensions of 3.0 X 0.254 mm, rests in a cylindrical alumina die

and an alumina punch presses the disk into the cavity as shown schematically in Fig. 2. The test apparatus installed in an environmental chamber is shown in Fig. 3. As shown, a water-cooled load cell was constructed inside the environmental chamber for accurate load measurement. The test is carried out in an inert atmosphere. Induction heating of a susceptor and subsequent conduction through the gas ensure uniform heating of the disk and ceramic workpieces. Permanently embedded thermocouples in the specimen support piece, which have been calibrated to the actual disk temperature, are used for temperature control and recording. During the test, either the applied load of the punch versus time under constant impression velocity or the punch displacement versus time under constant applied load are measured. Further design details regarding the MDBT apparatus were reported in Refs. 9, 10, and 11.

Experimental reproducibility for ten separate tests at room temperature is shown in Fig. 4. The material tested was nuclear grade Type 316 stainless steel with 20% cold work[a] (CW), otherwise known as N-LOT material in the breeder reactor alloy development arena. This material was chosen because the mechanical behavior has been well characterized and should serve as a good validation of the MDBT methodology.

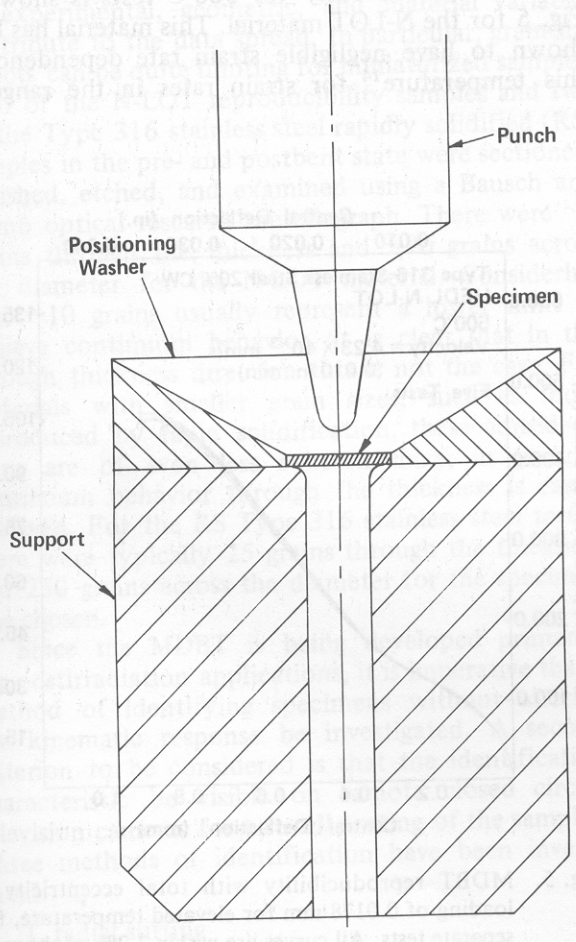

Fig. 2. Schematic of MDBT showing simply supported central loading.

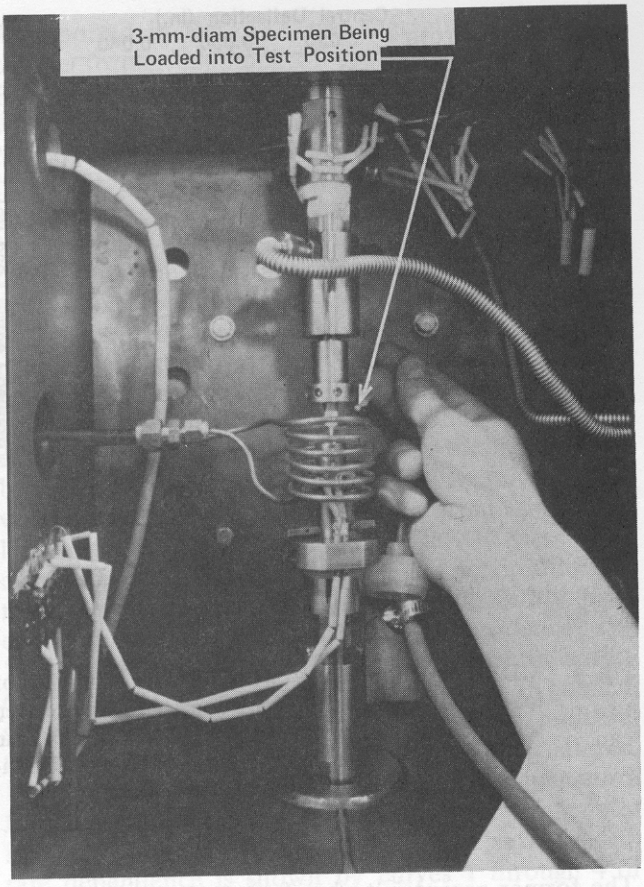

Fig. 3. Actual MDBT apparatus installed in environmental chamber. Specimen being positioned in preparation for elevated temperature test.

Alignment of the punch and die as well as specimen centering are critical since disk stiffness increases with eccentricity of loading. There are two basic contributions to total eccentricity that are of prime importance:

1. punch axis of symmetry not coincident with die axis of symmetry
2. design tolerance for die, positioning washer, upper disk support structure, and specimen outer diameter.

[a]Material obtained from Hanford Engineering Development Laboratory (HEDL) in a 0.348-mm-thick rolled sheet; heat designation 87210; HEDL N-LOT.

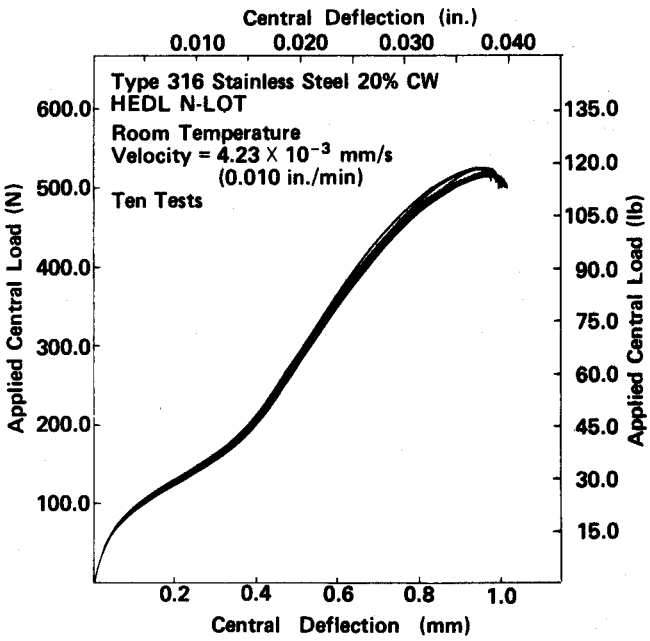

Fig. 4. MDBT reproducibility with total eccentricity of loading of 0.0178 mm for room temperature, ten separate tests. All curves are within 2.4% of the mean along the entire curve to the point of fracture initiation.

The former eccentricity has been reduced by using a precision alignment fixture, and the latter, by careful experimentation and by accurate machining of key components. The total eccentricity of loading was measured and found to be ~0.0178 mm for all the curves in Fig. 4. This measurement was made by placing a polished specimen in the die after alignment, applying a small load on the specimen, and subsequently measuring the location of the punch plastic indentation center and the die plastic indentation ring in an optical comparator. For this eccentricity, the central load/deflection curves for the ten tests fell within a band that is only 2.4% of the mean along the entire curve to the point of fracture initiation.

The central load/deflection reproducibility with 0.0178-mm eccentricity is as good as or slightly better than that normally attainable in conventional mechanical behavior testing of materials from a given heat. The American Society for Testing and Materials (ASTM) is developing quantitative estimates of the precision and accuracy of the methods set forth in Standard E8 (see Ref. 12). The ASTM currently advises that statements on accuracy should be limited to the documented performance of particular laboratories. Reference 13 reported axial tensile data for Fast Test Reactor prototypic fuel-cladding lots. Nine tests at room temperature were listed for the N-LOT material. For purposes of comparison with the MDBT data, the 95% confidence limits for the mean assuming a normal distribution reported in Ref. 13 for the 0.2% yield stress and the engineering ultimate tensile strength (UTS) were analyzed. The confidence limits were reported to be ±5.41% of the mean for the 0.2% yield stress, and ±2.0% of the mean for the UTS. Likewise, 95% confidence limits for the load response were calculated using the MDBT data in Fig. 4 for central deflections of 0.13 and 0.64 mm. As discussed in Sec. VII, the loads that correspond to these deflections are the loads that approximately correspond to the yield stress and UTS. The confidence limits were found to be ±4.62 and ±3.61% of the mean, respectively. The overall accuracy of the MDBT methodology is discussed in detail in Sec. V where sensitivity analysis results are presented. In essence, the comparable or slightly improved MDBT experimental accuracy is necessary to obtain stress/strain information of comparable accuracy to uniaxial tensile stress/strain information. The improved experimental accuracy in the MDBT is probably due to tight machining tolerances for specimens and apparatus as well as the MDBT loading configuration where no gripping extensions are necessary.

The reproducibility for 500°C tests is shown in Fig. 5 for the N-LOT material. This material has been shown to have negligible strain rate dependence at this temperature[14] for strain rates in the range of

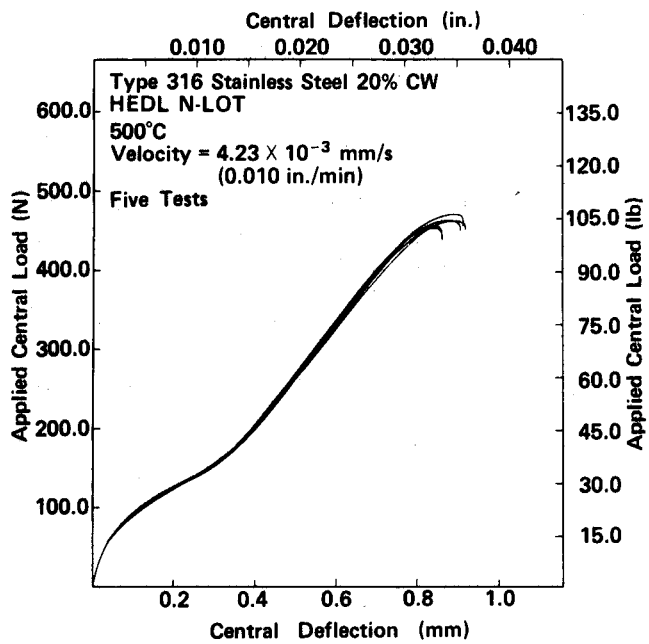

Fig. 5. MDBT reproducibility with total eccentricity of loading of 0.0178 mm for elevated temperature, five separate tests. All curves are within 3.2% of the mean along the entire curve to the point of fracture initiation.

10^{-5} to 10 s^{-1} and, therefore, a convenient punch velocity of 4.23 X 10^{-3} mm/s was chosen. This velocity corresponds to a strain rate of $\sim 10^{-1}\ s^{-1}$. The total eccentricity was ~0.0178 mm and the five central load/deflection curves all fell within 1.85% of the mean for a central deflection of 0.13 mm and 3.23% of the mean for a central deflection of 0.64 mm. The 95% confidence limits for the mean reported in Ref. 13 for the 0.2% yield stress and the UTS at 482°C are ±8.13 and ±3.41%, respectively. The 95% confidence limits for the load response were calculated using the data in Fig. 5 at the point of departure from linearity and for a central deflection of 0.64 mm and were found to be ±6.69 and ±2.85% of the mean, respectively. These confidence limits were calculated in the same way the Fig. 4 confidence limits were calculated. Experimental reproducibility for the MDBT in general has been judged to be quite good and total eccentricities of <0.0254 mm are readily achievable in practice and produce errors in test results that are comparable to or less than other experimental and analytical modeling uncertainties.

Demonstration of elevated temperature reproducibility is, of course, of prime importance since all experimental, geometric, and material variables contribute to the data spread. In particular, grain-size effects can be quite limiting for miniaturized samples. Two of the N-LOT reproducibility samples and two of the Type 316 stainless steel rapidly solidified (RS) samples in the pre- and postbent state were sectioned, polished, etched, and examined using a Bausch and Lomb optical research metallograph. There were ~6 grains through the thickness and ~70 grains across the diameter for the N-LOT material. Considering that ~10 grains usually represent a lower limit to achieve continuum behavior, it is clear that in the through thickness direction this is not the case. For materials with smaller grain sizes, such as those reproduced by rapid solidification, these considerations are of even less concern since, in general, continuum behavior through the thickness is easily achieved. For the RS Type 316 stainless steel tested there were typically 25 grains through the thickness and 250 grains across the diameter for the specimen size chosen.

Since the MDBT is being developed primarily for postirradiation applications, it is imperative that a method of identifying specimens without altering the kinematic response be investigated. A second criterion to be considered is that the identification characteristic be visible on remote closed circuit television cameras for hot-cell sorting of the samples. Three methods of identification have been investigated:

1. radial slitting
2. stylus engraving
3. laser engraving.

As reported in Ref. 11, laser engraving is preferable to the former methods of specimen identification. Radial slitting removes material from the outer edge, which results in a decrease in plate stiffness. This method has been abandoned for all future irradiations. Stylus engraving ploughs the material and leaves a track with a material lip protruding above the specimen surface. Laser engraving exfoliates the material by ablation and also leaves a track with a protruding lip. In general, stylus engraving is acceptable provided the character tracks are relatively narrow and shallow. Wide and deep tracks cause a plate stiffness reduction. However, one-sided laser engraving is somewhat more desirable because the exfoliated lip height is greater than the lip obtained by shallow stylus tracks and is therefore more visible for hot-cell sorting after irradiation. The laser-engraved tracks reported in Ref. 11 were sufficiently narrow and shallow that the load/deflection response curves fell within the reproducibility band of the unmarked specimens.

Experiments were performed to assess the ability of the MDBT to resolve strain rate effects. In general, strain rate dependence is observed at high temperatures and low strain rates. For the N-LOT material, Ref. 14 reported negligible strain rate dependence for temperatures below ~650°C, and for strain rates in excess of $\sim 10^{-3}\ s^{-1}$ at 650°C. This lack of strain rate dependence is shown by curves 1 through 4 of Fig. 6 for the N-LOT material. Also, the ability of the MDBT to clearly resolve strain rate effects is demonstrated by curves 5 and 6 in Fig. 6.

For uniaxial tensile testing, the strain rate is clearly defined and is directly proportional to velocity. However, in the MDBT, because of the nonuniform biaxial stress field, it is not possible to obtain a simple analytical formula relating velocity to instantaneous strain rate. Also, the instantaneous strain rate varies throughout the plate as the deformation proceeds. The approximate definition of average strain rate adopted is

$$\bar{\dot{\epsilon}} \approx \frac{\Delta \epsilon_u}{\Delta t_u} = \frac{(\Delta \epsilon_u) v}{w_u} \quad , \tag{1}$$

where

$\bar{\dot{\epsilon}}$ = average MDBT strain rate

Δt_u = time to reach maximum central load

v = punch velocity

w_u = central deflection at maximum load

$\Delta \epsilon_u$ = uniform uniaxial or equivalent biaxial strain.

This is the relation that was used to determine the average strain rates in Fig. 6 since the uniform uniaxial strain was known beforehand for the N-LOT material. This approximation is certainly correct to

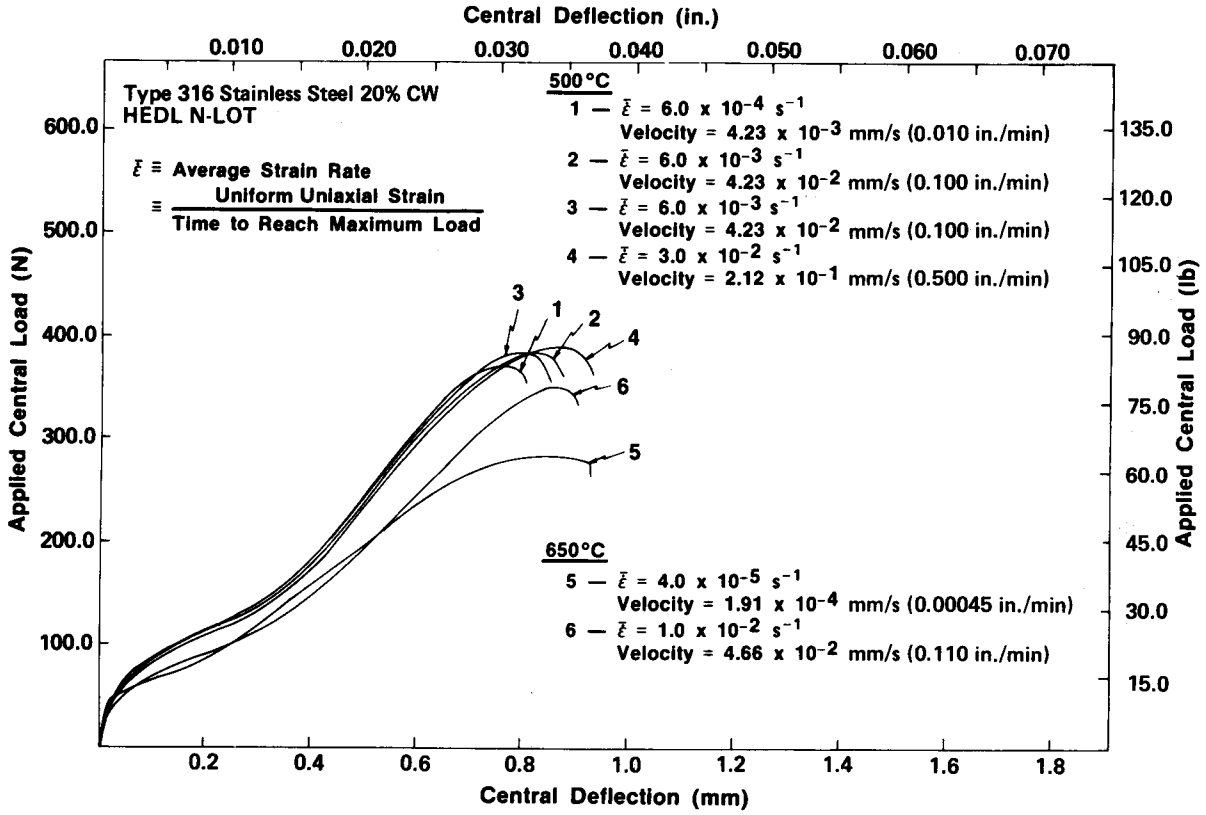

Fig. 6. Demonstration of MDBT ability to resolve strain rate effects.

within an order of magnitude and probably within a factor of 2 as an estimate of the average strain rate in the sample throughout the deformation process. For materials with unknown mechanical behavior, it is necessary first to perform the finite element data inversion to obtain the uniform strain, and then determine the average strain rate during the test. An alternative definition, which would provide an estimate of the average strain rate prior to data inversion, is

$$\bar{\dot{\varepsilon}} \approx \frac{\Delta\epsilon_y}{\Delta t_y} = \frac{(\Delta\epsilon_y)v}{w_y} , \qquad (2)$$

where

Δt_y = time to reach point of departure from linearity on central load/deflection curve

w_y = deflection to reach point of departure from linearity on central load/deflection curve

v = punch velocity

$\Delta\epsilon_y$ = yield strain or 0.002.

The ability of the MDBT to experimentally resolve different materials as well as differences in thermomechanical treatment (TMT) for materials of the same base alloy has been demonstrated.[9,10] Central load/deflection curves for a variety of materials and processing conditions were reported, and each material had unique and distinguishable central load/deflection curves. This was also true for cases where TMT is the only difference. Figure 7 illustrates the wide range of ductility variation that can be experimentally resolved by the MDBT procedure.

III. FINITE ELEMENT MODELING

Finite element analysis is performed to convert the experimental central load/deflection curves into stress/strain and ductility information. To accurately analyze the MDBT using the finite element method, a new finite element frictional contact boundary condition model has been developed.[9] The strain field present in the MDBT is highly nonuniform throughout the sample, unlike the more conventional uniaxial tensile strain fields, which are constant (in the gauge section) for a given static load up to the point of plastic instability. Therefore, accurate three-dimensional boundary condition modeling is essential in simulating the actual strain gradients in the specimen during the experiment. The model accounts for this highly nonlinear boundary value problem with shifting frictional contacts.

The MDBT problem contains all three types of

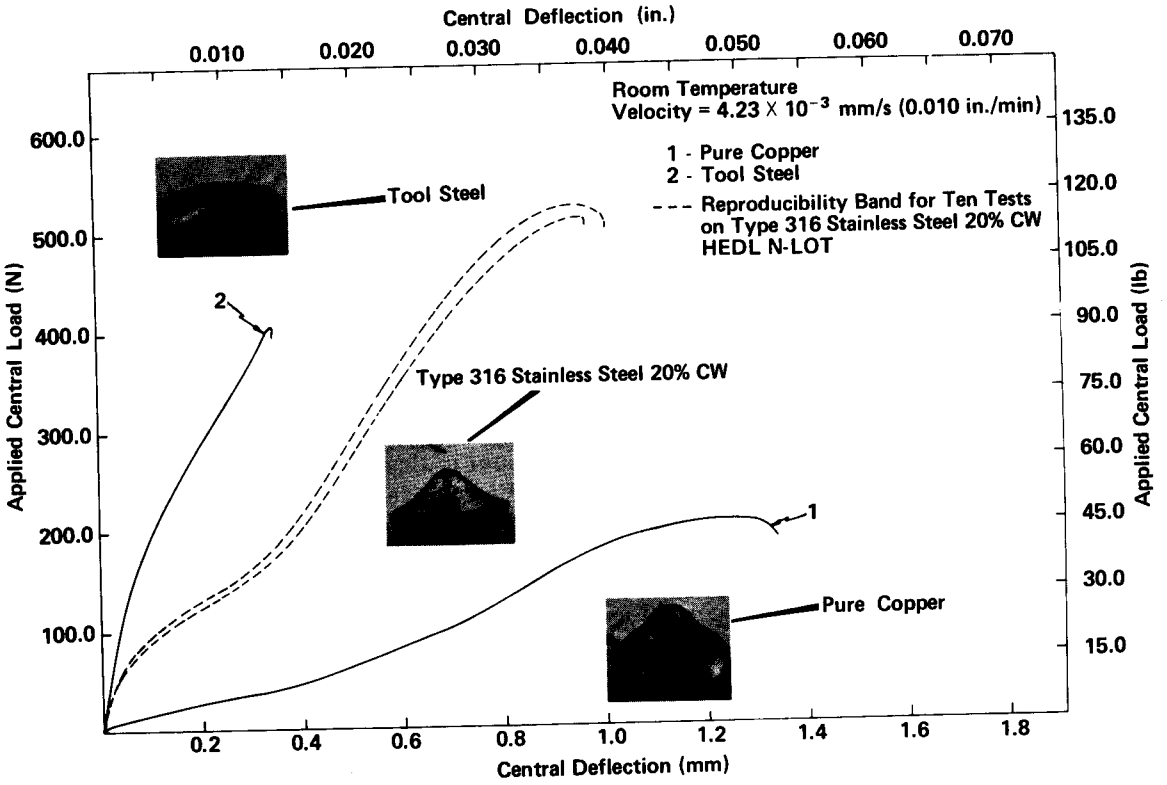

Fig. 7. MDBT experimental results for materials with widely differing ductilities.

nonlinearity that can be encountered in stress analysis, namely, material, geometric, and boundary. The first two classifications of nonlinearity have been quite adequately addressed in several general purpose finite element codes.[15,16] The latter classification of nonlinearity has not been adequately addressed to date, and therefore a new finite element friction-gap boundary condition model has been developed. Although the model has been applied to the MDBT problem in particular, the method developed is of general applicability to a wide variety of boundary condition problems.

Various methods to deal with friction in the finite element method have been proposed over the past 10 yr, primarily for application in the metals-forming industry. Nagamatsu et al.[17,18] introduced a slip factor that is used to modify surface nodal displacements. Gordon and Weinstein,[19] Iwata et al.,[20] and Odell[21] imposed surface nodal forces that are oppositely directed to the nodal displacement direction. A similar technique for opposing surface nodal displacement was proposed by Shah and Kobayashi[22] and Matsumoto et al.[23] by introducing a surface shear stress that is evaluated from an empirical constant. As formulated by these authors, both the force method and the surface shear stress method are only applicable to problems where the direction of nodal displacement is known prior to the start of the analysis. Sharman[24] and Zienkiewicz et al.[25] proposed interfacial friction elements for very small deformations, which do not require prior knowledge of the direction of nodal displacements, and utilized them successfully for very small deformations. Hartley et al.[26] extended this idea to include large deformations. They found that for relatively small deformations the interfacial element layer exhibits unstable deformation and subsequently collapses. They circumvented this difficulty by introducing an element layer stiffness modifying function that depends on the ratio of the yield stress of the surface layer to that of the bulk material. The technique was applied to ring compression and satisfactory results were achieved. Although this method appears promising for simple geometries, the validity of this approach has yet to be demonstrated for complex loading geometries. Also, this method, as currently formulated, does not account for shifting contact during the deformation process. Thus, it is obvious that a new finite element friction model development, which does not depend on prior knowledge of the deformation kinematics and accounts for shifting contact, is necessary.

The ABAQUS computer code[16] was chosen for this modeling application because of its superior nonlinear capabilities. Some of the more important capabilities necessary to adequately model the MDBT

nonlinear boundary value problem are two-dimensional axisymetric continuum elements, multilinear material hardening, large rotations/large displacements, and finite strains. ABAQUS currently has all of these capabilities with the exception of finite-strain theory. However, this capability is currently being added to the code and will be available in the near future. The code now implements small-strain theory with large rotations and large displacements. Roadal recently compared finite-strain theory with small-strain theory.[27] He compared these two formulations for thin structures (such as beams, rings, and plates) and concluded that large differences between the finite-strain theory and small-strain theory results exist for strains greater than ~5.0% or larger. These differences were found primarily at regions where large strain gradients occur. However, for high-fluence postirradiation materials investigations at elevated temperatures, the small-strain theory may prove adequate in many instances since the ductility of many materials under these conditions is greatly reduced.

Another very important aspect of the ABAQUS code is the fact that it already contains a simple two-body dual node friction model applicable to Cartesian space. The code uses classical Coulomb friction with a stiffness in stick method to aid convergence. This simple model can be used as a basic building block to accurately represent multiple node frictional contact boundary conditions for essentially any geometry by the introduction of the shadow node concept. This theory enables mapping of the region of contact between a support and a deforming structure in contact with it from two-dimensional cylindrical space, for example, to two-dimensional Cartesian space where the code can solve the friction problem. The details of this new theoretical development are beyond the scope of this paper and will be presented elsewhere. It will suffice here to provide a qualitative description of the model. In essence, two fictitious shadow nodes are introduced into the analysis, somewhere in Cartesian space, for every real physical node in the plate that is a potential contact/friction node. One of the shadow nodes models the plate while the other models the deforming structure. Multipoint constraint equations are written to eliminate the plate shadow node degrees of freedom. In this fashion, the friction-gap problem is effectively mapped from two-dimensional cylindrical space to two-dimensional Cartesian space where the code can model two-body dual node friction. Since the method operates directly on the plate nodes, it can therefore be termed a direct boundary condition method as opposed to the indirect methods, which use interfacial elements. The method is implemented in such a way that the frictional forces always oppose the direction of nodal displacement since we map the slip displacements to Cartesian space as well. Therefore, when a node changes direction, the nodal surface force automatically changes sign. Also, there are no kinematic assumptions on the deformation other than the fact that a plate node cannot penetrate the punch or support region. Therefore, a solution correct to within the limitations of continuum mechanics is obtained. In this modeling application, the punch and the support were taken to be infinitely rigid. Since the MDBT has been principally designed to test metallic materials at elevated temperatures, this is a reasonable assumption. However, in the future, equations could be written to relax this assumption. Phenomena such as separation of the punch and plate near the center are automatically taken into account in this model.

Eight-noded two-dimensional axisymmetric continuum elements were used for analysis of the MDBT experiment. Isotropic hardening with a von Mises yield function was used in all analyses. In the isotropic formulation, the code requires the tangent modulus. Therefore, the uniaxial work hardening curves are multilinearized. Since all elements in the plate are initially rectangular, reduced integration was used to take advantage of superconvergence.

Limit analysis studies were performed to test the friction-gap model. The support model was activated and an elastic solution performed for a point-loaded plate. A 20-element mesh, which consists of 2 elements through the thickness and 10 elements along a radius, was used. The true elastic plate response lies between two bounds:

1. a roller support that corresponds to a friction coefficient of zero
2. a fixed node support that corresponds to an infinitely large coefficient of friction

As anticipated, the results using the friction-gap support model with zero and infinitely large friction coefficients were identical to the results obtained using roller support and fixed node support boundary conditions, respectively.

A mesh refinement study was performed to verify that the 20-element mesh is sufficiently refined. A 100-element mesh was run and the solution compared with the 20-element mesh solution. The 100-element mesh consisted of 4 elements through the thickness and 25 along a radius. The results were essentially identical away from the punch. Near the punch, the solutions differed somewhat because the boundary conditions were different. The 100-element model is inherently less stiff and also has more potential friction nodes per unit surface length. This results, in general, in more punch surface contact with the plate for a given static load. There were some slight differences in the central load/deflection response, and these will be discussed in

detail in Sec. IV. The 20-element mesh was judged adequate from a mesh refinement standpoint and was used in all subsequent analyses. In future analyses, local mesh refinement is recommended near the punch contact region in order to get more accurate strain distributions for cases where biaxial stress information is desired. A typical deformed plate configuration superimposed on the undeformed configuration is shown in Fig. 8 for a punch deflection of 0.254 mm. The equivalent plastic strain contour for this punch deflection is shown in Fig. 9.

The friction coefficient for clean stainless steel on clean high-density alumina lies between ~0.2 and 0.6, and a value of 0.4 was used in all analyses reported herein. The friction coefficient can be treated as a tuneable parameter for the purpose of data inversion, unless it is carefully measured for the materials and surface conditions present in the experiment. If the friction coefficient is not measured, an estimate for a given class of materials can be obtained by testing a material with known mechanical behavior. The finite element code is then run several times to determine the friction coefficient. The value of 0.4 for the friction coefficient used in the analyses reported herein yields excellent agreement between the finite element results and the experimental data. In the future, sensitivity analyses could be done to estimate the impact of changes in the friction coefficient on mechanical behavior determination. The mean coefficient of friction has been shown to be approximately temperature insensitive for temperature variations that merely affect the mechanical strengths of the two bodies.[28] This is because the shear strength and hardness of the weaker material in contact are affected to about the same degree. Since the MDBT testing is done in inert atmosphere, to first order, the assumption of no temperature dependence of the friction coefficient is valid.

IV. DEMONSTRATION OF VALIDITY OF METHODOLOGY

The validity of the MDBT methodology must be demonstrated for a material with well-characterized mechanical behavior before it can be safely used in practice. The Type 316 stainless steel 20% CW N-LOT material was chosen for this purpose. Of course, once this is accomplished, the MDBT can be used to determine mechanical behavior. The problem at hand, therefore, reduces to that of generating a central load/deflection curve using the finite element method that matches the experimental data presented in Fig. 5.

The known uniaxial tensile behavior at 482°C of the N-LOT material[13,29] was used as code input. These data were piecewise linearized as shown in

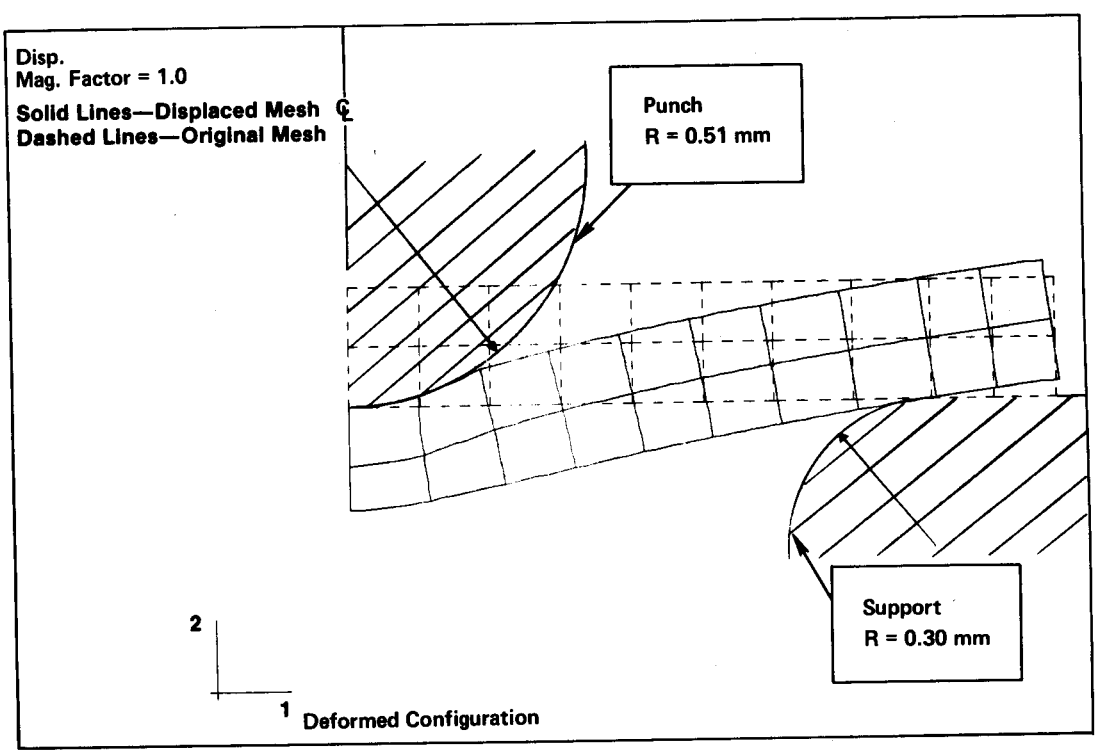

Fig. 8. Calculated deformed configuration for punch displacement of 0.254 mm.

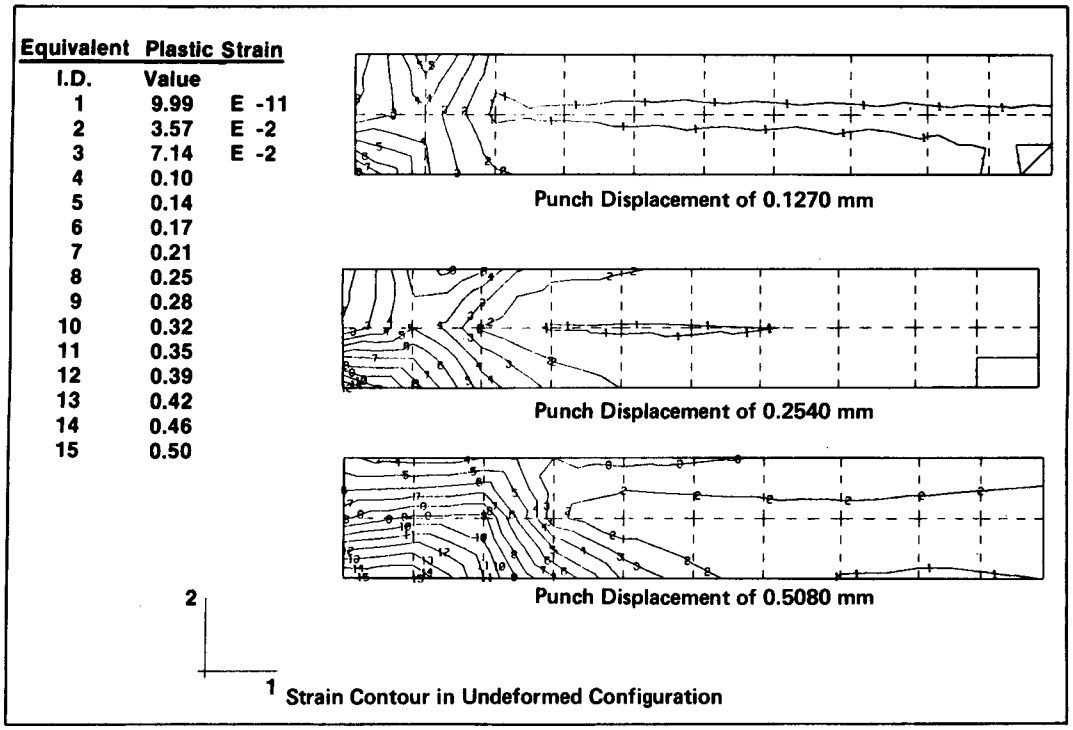

Fig. 9. Calculated equivalent total plastic strain contours for various punch displacements.

Fig. 10. A 20- and a 100-element mesh were run. The applied central load and deflection output are plotted with the Fig. 5 experimental reproducibility band in Fig. 11. The finite element prediction is quite accurate up to a central deflection of ~0.45 mm. The force balance tolerance provides an estimate of the central deflection beyond which small-strain theory is no longer valid. As shown in Fig. 11, the convergence tolerance becomes sizable after a central deflection of ~0.45 mm for the 100-element mesh. One of the bottom elements near the plate center actually turns in on itself at this deflection magnitude. This explains the large force balance tolerance for the 100-element mesh after central deflections of 0.45 mm. Since there are only two elements through the thickness for the 20-element mesh, this phenomenon occurs at a larger central deflection for this mesh. Therefore, as anticipated, for materials which exhibit large ductility, the finite-strain theory must be implemented.

As discussed in Sec. III, the friction-gap model developed is a discrete model. This explains why the 100-element mesh gives a better load prediction at a central deflection of 0.13 mm as shown in Fig. 11. At a central deflection of 0.15 mm, the 20-element mesh solution agrees with the 100-element mesh solution because another plate node has come into contact

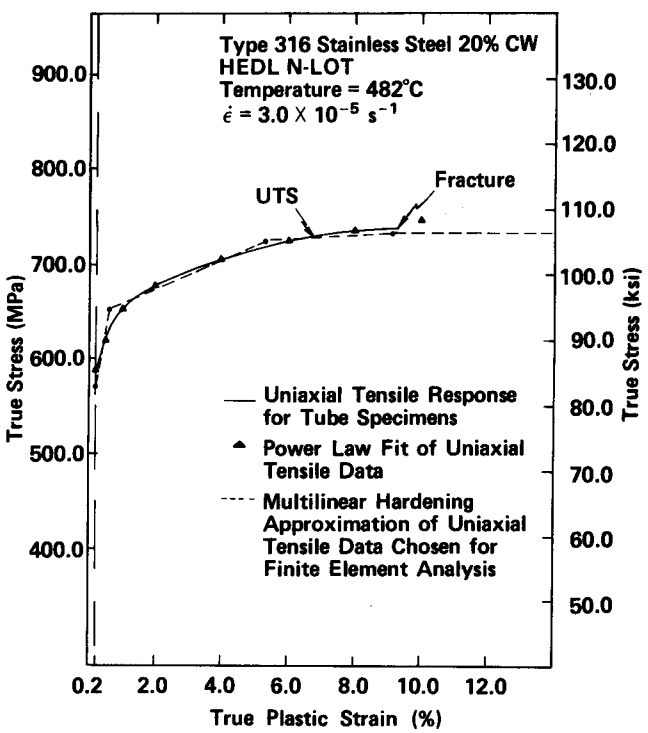

Fig. 10. Uniaxial tensile data for Type 316 stainless steel 20% CW (HEDL N-LOT material) at 482°C.

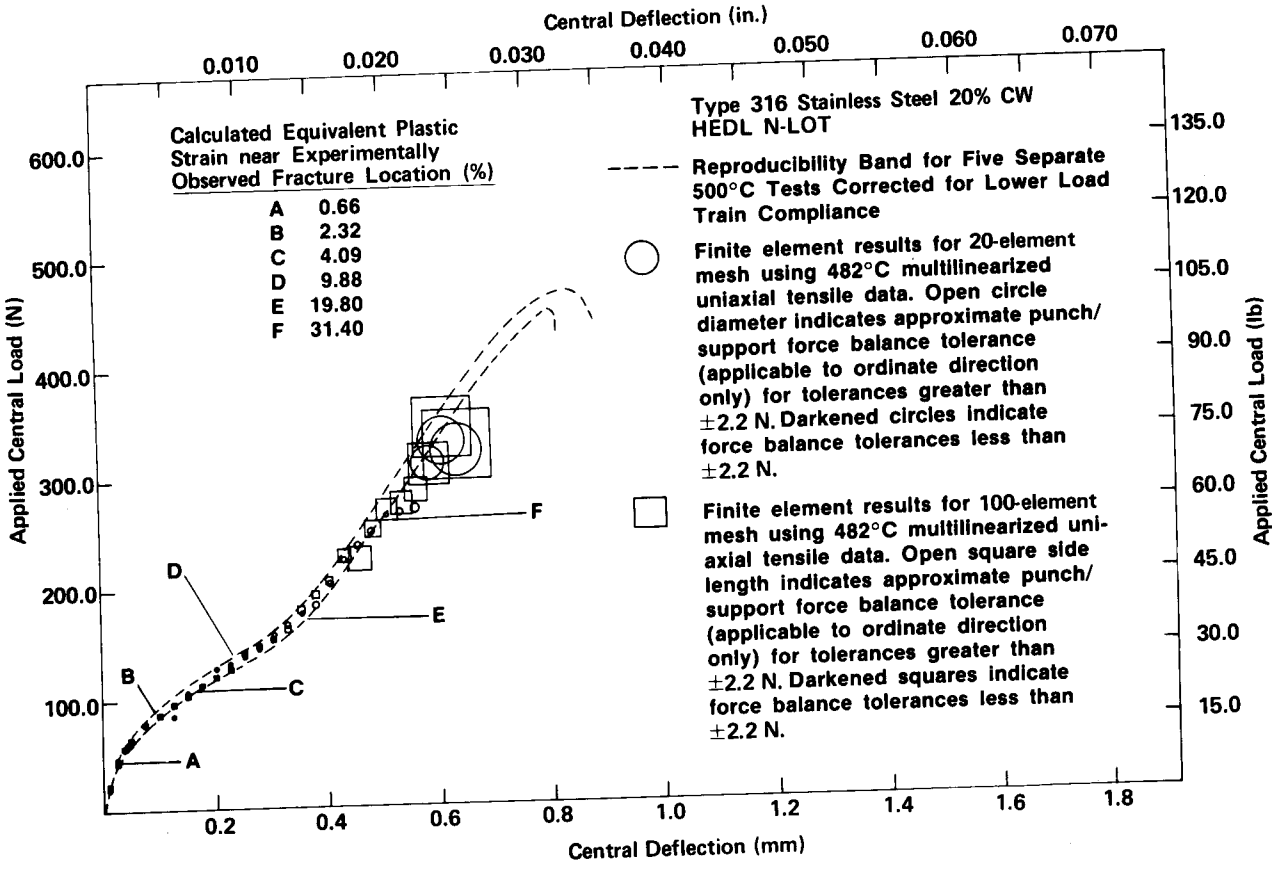

Fig. 11. Demonstration of validity of MDBT methodology. Finite element solution generated using known uniaxial stress/strain behavior shows excellent agreement with MDBT data.

with the punch. The 100-element mesh has more area in contact with the punch, in general, than the 20-element mesh and more accurately models the loading and propagation of the annular contact region along the punch surface as the deformation proceeds. The loading condition is obviously different in the two meshes, which thus affects the strain distribution near the punch. However, the 20-element mesh strain distribution is similar to that calculated using the 100-element mesh away from the punch. Therefore, if uniaxial material behavior of an irradiated material is desired, the 20-element mesh is adequate and more cost effective than the 100-element mesh. However, if biaxial stress/strain information near the point in the plate where fracture initiation is experimentally observed is desired, then local mesh refinement near the punch tip is necessary for future analyses. The 100-element mesh requires ~4 to 5 times more running time than the 20-element mesh.

The through thickness fiber rotations near the support are initially larger than the tendency of the plate to draw into the die, which results in the bottom surface nodes displacing a small distance radially outward initially. At higher levels of deformation, these nodes reverse their directions and displace radially inward. The friction model automatically changes the sign of the surface friction force when node direction reversal occurs. Also, the finite element solution shows that all plate material points remain within a 3.0226-mm-diam cylindrical space throughout the entire deformation for an undeformed 3.0-mm-diam disk. This cylindrical region is adequate to ensure that the specimen will drop into place in the positioning washer located in the disk support piece. This information may be useful in future designs to minimize the tolerance between the specimen and positioning washer in the experiment to provide better alignment and also maintain the simply supported boundary condition. The model also predicts separation of the punch from the plate at the center leaving an annular section in contact for a punch displacement in excess of 0.15 mm. Experimental evidence of this phenomenon was discussed in Refs. 9 and 10. In general, excellent agreement between the finite element prediction and experimental data has been observed.

V. EXPERIMENTAL DATA INVERSION ACCURACY

An analysis was performed to gain some understanding of the resolution capability of the MDBT methodology as compared to the more conventional approach of uniaxial tensile testing to determine mechanical behavior. The multilinearized work-hardening curve for the N-LOT material at 482°C shown in Fig. 10 was increased by 2 and 10%, respectively, for a given strain level, as shown in Fig. 12. For ease of discussion, these two cases will be loosely referred to as the 2 and the 10% flow stress input changes, respectively. The 20-element mesh was used to determine central load and displacement information. The calculated central load/deflection curves are presented in Fig. 13. It is clear from the figure that curves 1 and 2, which are the results for the 0 and the 2% flow stress input changes, respectively, fall within the experimental reproducibility band. However, curve 3 in Fig. 13, which represents the 10% flow stress input change, lies well above the experimental reproducibility band. Therefore, the stress/strain resolution capability of the MDBT methodology lies somewhere between a 2 and 10% flow stress input variation.

To gain a more quantitative understanding of the

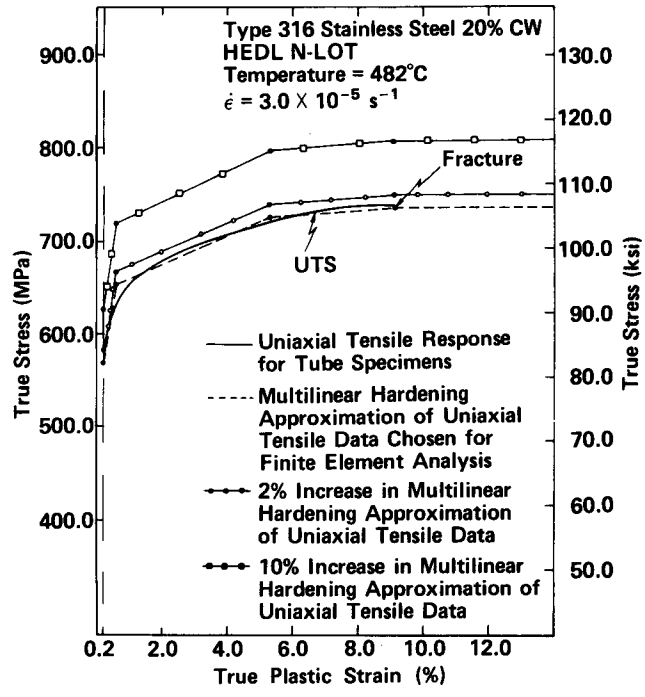

Fig. 12. Multilinear hardening approximation of flow curve varied by 2 and 10%, respectively, to assess MDBT stress/strain resolution capability.

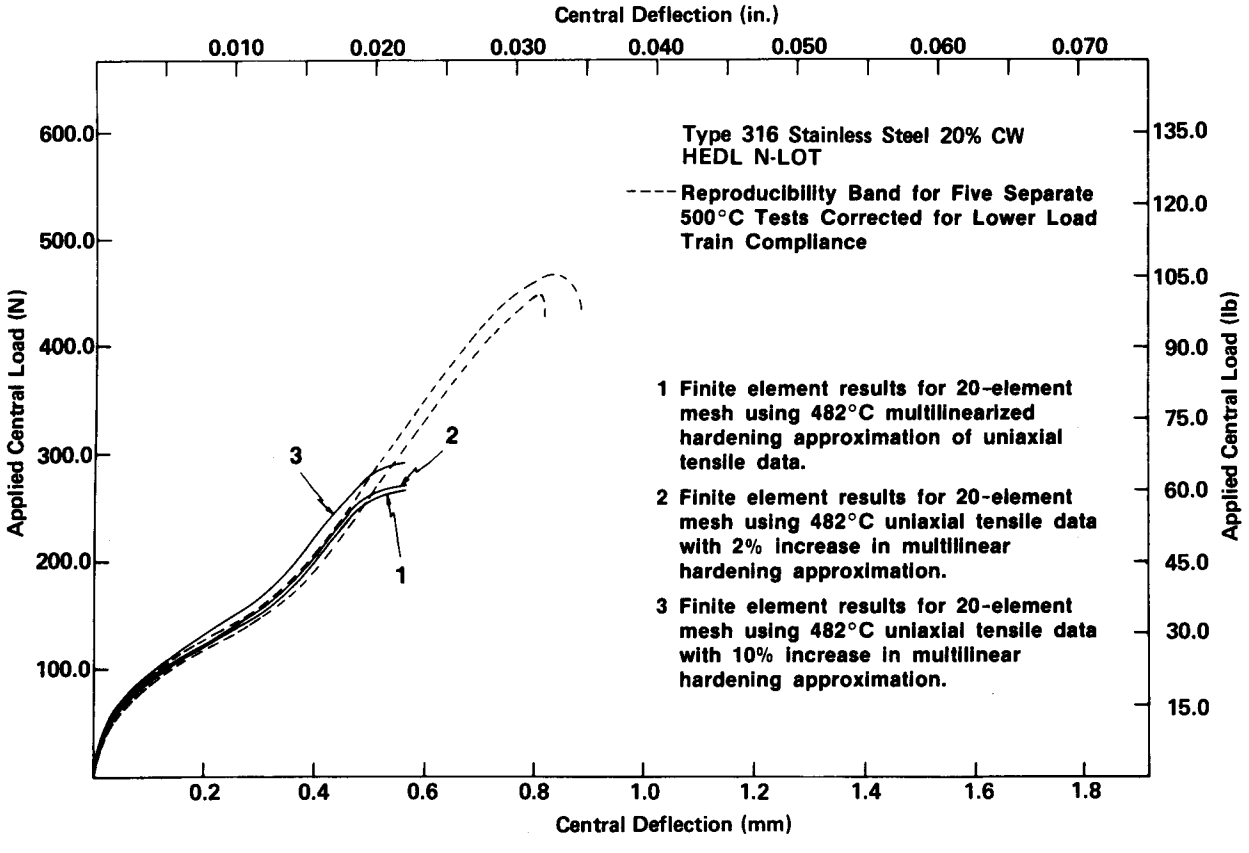

Fig. 13. Calculated applied central load/deflection curves for 2 and 10% change in flow curve compared to experimental reproducibility band.

MDBT stress/strain determination accuracy, the percent change in calculated applied central load was plotted against the normalized central deflection for the 2 and 10% flow stress input changes as shown in Fig. 14. The reason for the large deviation from the mean percent calculated load shown in Fig. 14 at normalized central deflections of 0.2 and 0.6 is due to the fact that the friction-gap model is discrete, and therefore the boundary conditions change significantly as additional nodes come into contact with the punch. A 2% change in flow stress input results in a mean percent calculated load change of ~1.8. Likewise, a 10% change in flow stress input results in a mean percent calculated load change of ~8.3. These results are plotted in Fig. 15. The resulting curve is approximately linear and is observed to lie very close to the unity slope line, which obviously indicates good inherent resolution capability for the MDBT methodology. If, for example, the slope of this line were significantly >1.0, then a small change in the load response would result in a large difference in the calculated stress. In this case, a small experimental error would result in a large uncertainty in the calculated stress/strain results. Fortunately, this is not the case. In essence, the nearly linear curve plotted in Fig. 15 indicates that it is possible to obtain reasonable accuracy in the MDBT stress/strain calculation provided the experimental error is sufficiently reduced.

The data inversion accuracy is now discussed and compared with the large sample data. Figure 15 can be thought of as an uncertainty mapping function from uniaxial tensile stress uncertainty space to the resulting MDBT applied central load uncertainty space, or vice versa. As discussed in Sec. II, Ref. 13 reported 95% confidence limits for the 0.2% yield stress and UTS of the N-LOT material at 482°C for nine separate uniaxial tensile tests on tube specimens. The 95% confidence limit for the 0.2% yield stress was ±8.13% of the mean and the 95% confidence limit for the UTS was ±3.41% of the mean. Using Fig. 15, these 95% confidence limits in stress map into maximum calculated changes in MDBT mean applied central loads of ±6.8 and ±2.75%, respectively. As discussed in Sec. II, 95% confidence limits for the MDBT applied central load were calculated for the N-LOT material at 500°C using the data shown in Fig. 5. The 95% confidence limit at the point of departure from linearity was found to be ±6.69% of the mean. This point on the central load/deflection curve corresponds to the 0.2% yield stress. Further discussion on the interpretation of the central load/deflection curve will be presented in Sec. VII. At a central deflection of 0.64 mm, the 95% confidence limit was found to be ±2.85% of the mean. This point on the central load/deflection curve approximately corresponds to the UTS. Again, using Fig. 15, these confidence limits are found to map into stress uncertainties of ±7.90 and ±2.50%, respectively. The confidence limit band width for uniaxial testing is primarily determined by material variability and experimental errors such as those introduced in specimen machining, gripping extensions, column alignment that can result in bending, and transducer

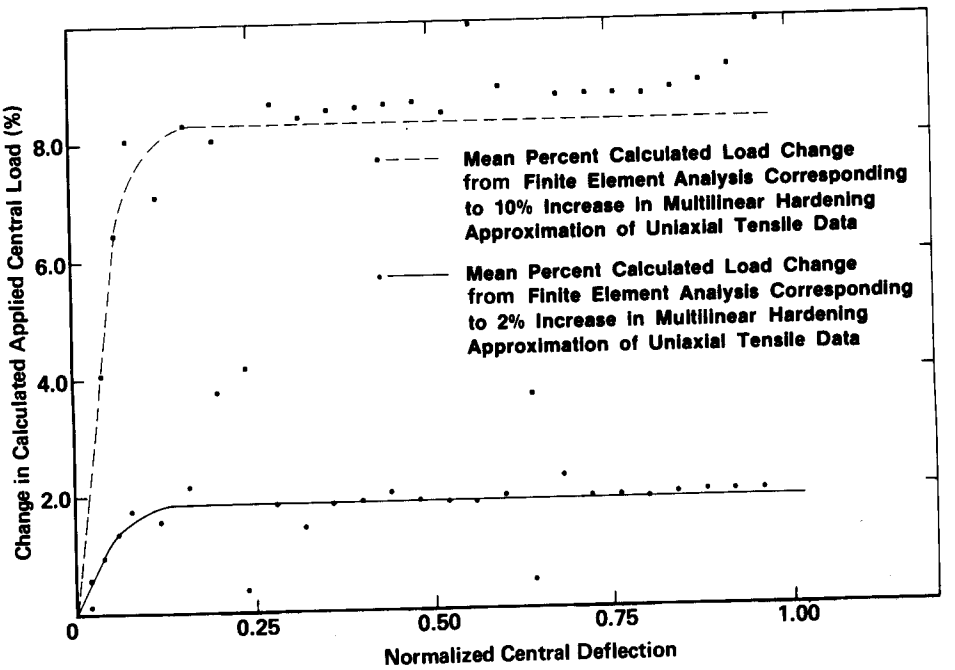

Fig. 14. Percent change in calculated applied central load for 2 and 10% change in flow curve input.

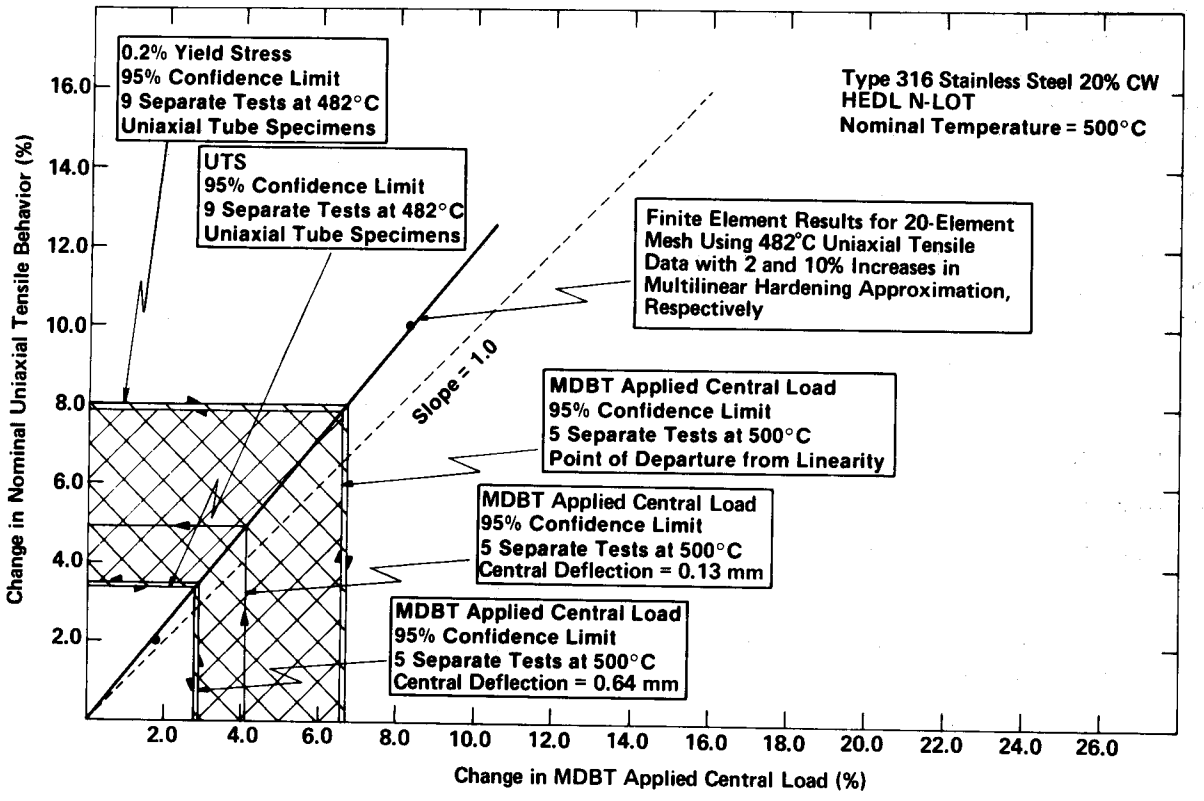

Fig. 15. Uncertainty mapping function from uniaxial tensile stress space to MDBT applied central load space.

accuracy. The confidence limit band width for the MDBT is primarily determined by material variability and experimental errors such as those introduced in specimen machining, friction coefficient variation, punch/die/specimen alignment, and transducer accuracy.

In summary, Fig. 15 indicates that the MDBT methodology is capable of delivering uniaxial work-hardening information with approximately the same level of accuracy as that present in the more conventional uniaxial tensile testing approach. In the future, more data should be taken to determine whether or not the MDBT is more accurate than uniaxial tensile testing since there are not enough uniaxial tensile data or MDBT data to ensure very accurate statistics. Also, the 95% confidence limits vary significantly with temperature for a given heat of material, and this effect can also be examined in future research. Nevertheless, these results on the MDBT resolution capability are quite encouraging.

VI. POSTIRRADIATION DATA INVERSION STRATEGY

The basic postirradiation data inversion strategy for the near term is

1. make informed guesses of several flow curves that bracket the flow curve of the material being investigated
2. implement the finite element code and generate central load/deflection curves for the various flow curves of step 1
3. compare finite element results with experimental data (repeat steps 1 and 2 until a calculated central load/deflection curve falls within the experimental reproducibility band).

This is a near-term strategy because in time the finite element data base will become sufficiently large, for a standardized specimen and loading geometry, that no further finite element runs will be necessary. In time, an interpolation routine can be written to invert the experimental data. To implement the near-term data inversion strategy effectively, a convenient method of parameterization of the flow curves is desirable. In general, an arbitrary flow curve can be multilinearized and input to the code. However, the most effective strategy is to use trial flow curves that are expressible as mathematical relations. In this way the shape of the trial flow curves can be limited to a narrow class of shapes. Care must be exercised in the choice of mathematical

representation to ensure that the material being tested actually performs in accordance with the choice of the shape function. Also, computing costs can be reduced by taking advantage of prior knowledge regarding the shape and expected behavior after irradiation (i.e., irradiation hardening or softening behavior, ductility reduction, etc.).

The flow curves of many materials from initial yield to the end of the region of uniform plastic deformation, and often beyond, can be approximated by a power law relation as

$$\sigma = K\epsilon^n \ , \tag{3}$$

where

σ = true stress

ϵ = true strain

n = strain-hardening exponent

K = strength coefficient.

The strength coefficient can be written in terms of the uniform stress and strain:

$$K = \frac{\sigma_{UTS}}{n^n} \ , \tag{4}$$

where σ_{UTS} is the true ultimate tensile strength.

Therefore, the entire flow curve can be parameterized by the true ultimate tensile strength and the true uniform strain. The yield stress is defined by cutting off the flow curve at 0.2% strain as illustrated in Fig. 10.

The material elastic stiffness is, of course, characterized by Young's modulus, which is primarily determined by atomic binding forces. The elastic modulus is, therefore, quite structure insensitive because the atomic binding forces cannot be significantly altered without modifying the basic nature of the material. Therefore, the Young's modulus can be determined to sufficient accuracy by testing a uniaxial specimen at temperature in the unirradiated condition. If a uniaxial test cannot be done, it is trivial to run an elastic finite element solution to determine Young's modulus. A preirradiation uniaxial test at temperature is advisable since the stress/strain curve generated, in general, provides a lower bound to the postirradiation stress/strain curve.

A variety of materials in the postirradiation condition were tested for irradiation experiments carried out in the High Flux Isotope Reactor (HFIR) at Oak Ridge National Laboratory (ORNL). The calculated irradiation parameters are listed in Table I. ORNL reported a potential error in the in-core temperatures for the CTR-32 experiment. Direct temperature measurements are not currently possible since HFIR was not initially designed for instrumented experiments. The temperatures reported were based on gamma-heating calculations. The gamma-heating rates in HFIR are quite high and the temperature gradients are rather steep. As a result, the temperatures reported previously by ORNL for HFIR may be ~50 to 75°C too high. However, the specimens were tested at the originally reported irradiation temperatures.

The pre- and postirradiation results for the Path A-1 RS material are shown in Figs. 16 and 17. The Path A-1 material is identical to primary candidate alloy of the national fusion alloy development program, which consists of titanium modification of nuclear grade Type 316 stainless steel.

As discussed in Sec. II, radial slitting can produce significant errors in the central load/deflection response. Therefore, preirradiation tests on slitted specimens were performed for comparison. Unfortunately, the radial slitting study results were not available prior to submitting the specimens for irradiation. Examination of Figs. 16 and 17 indicates that for the materials tested the slits can produce significant effects on the central load/deflection response at room temperature as expected. However, the effects are not as dramatic at elevated temperatures where the material flows more readily. Therefore, although not exact, the elevated temperature data for the postirradiated samples are fairly close to the response obtained for samples without radial slits.

In the analyses reported herein, the work-hardening relationships before and after irradiation were assumed *a priori* to be of the same shape. This assumption is shown to be reasonable for the materials examined; however, this assumption will not

TABLE I

HFIR CTR-32 Calculated Irradiation Parameters

In-Core Position	Temperature (°C)	Fast Fluence (0.1 meV n/m^2)	Thermal Fluence (n/m^2)	Total Fluence (n/m^2)	dpa (Type 316 Stainless Steel)	Helium (12.4% nickel) (at. ppm)
4	600	1.1×10^{26}	2.1×10^{26}	4.4×10^{26}	8.5	360
9	500	1.1×10^{26}	2.1×10^{26}	4.4×10^{26}	8.5	360

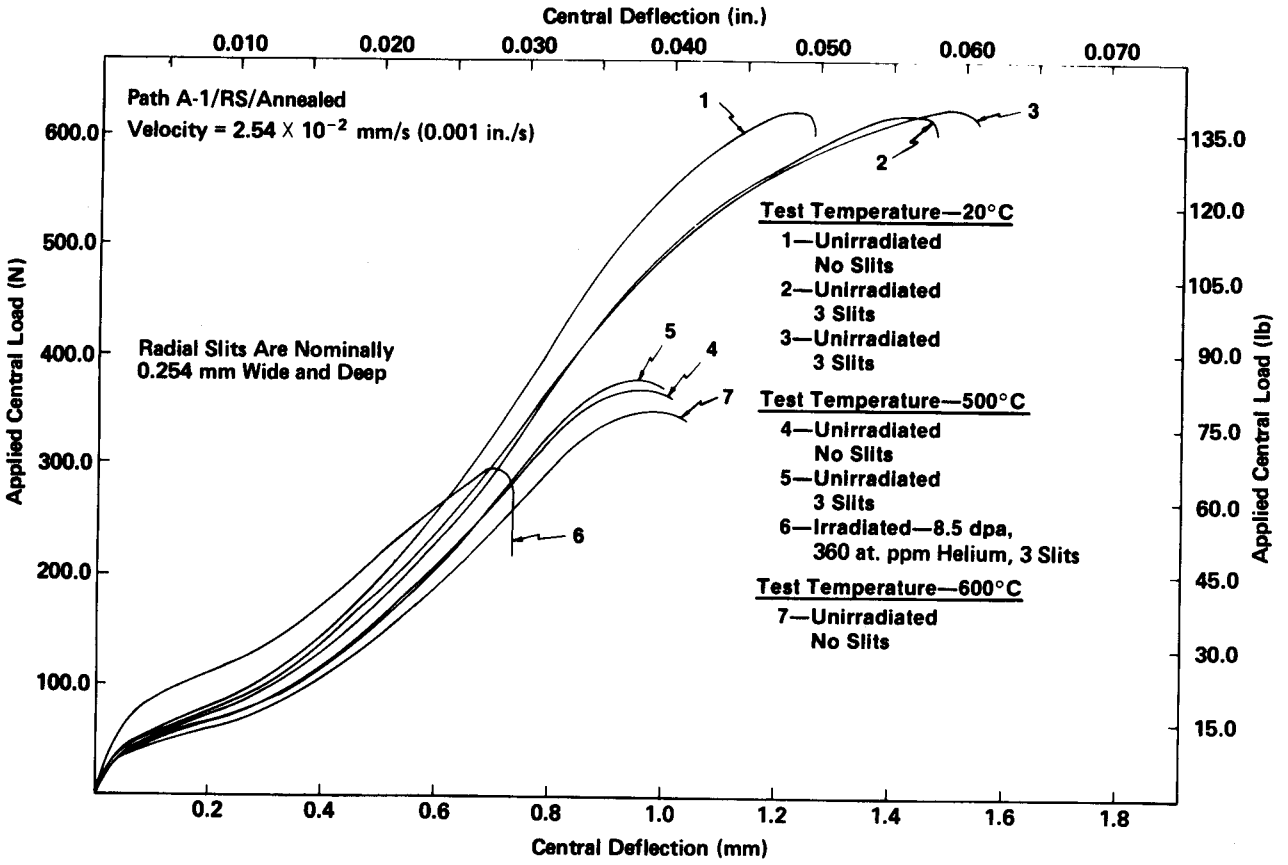

Fig. 16. Postirradiation data for Path A-1/RS/annealed material.

hold in all cases. In future materials testing, it will be useful to gain experience using alternative mathematical relations for the work-hardening curves.

The parameterized spectrum of flow curves analyzed is shown in Fig. 18. The resulting central load/deflection curves generated using the various flow curves are presented in Fig. 19. Figure 19 is repeated in Fig. 20 with the postirradiation Path A-1/RS experimental curves superimposed. The Path A-1/RS/20% CW experimental data are best matched by curve 5 in Fig. 20, and the Path A-1/RS/Annealed experimental data are best matched by curve 6 in Fig. 20. However, these results are only approximate because of inherent experimental inaccuracies (such as specimen slitting) present in the experimental data for this group of postirradiated specimens.

VII. FUNDAMENTAL INTERPRETATION OF EXPERIMENTAL DATA

Analyses were performed to provide a fundamental interpretation of the applied central load/deflection curves. As illustrated in Fig. 21, the central load deflection curve can be divided into five distinct regions each of which is primarily governed by widely differing modes of deformation and phenomena.

Examination of the strain contours reveals that the plate yields upon contact with the punch in a localized region near the punch tip. However, over the initial linear portion of the load/deflection curve, which spans the first 0.0381 mm of deflection, the bulk of the plate response is in the elastic regime. This has been verified in the finite element analyses and also experimentally by loading and unloading several times up to the point of departure from linearity on the load/deflection curve. During these experiments, the linear portion of the curve was retraced until bulk plate yielding occurred at the point of departure from linearity. Also, a small plastic indentation at the center of the plate where the punch made contact was observed for all loading in the bulk plate elastic range.

During the deformation in region 1, the yield surface in the plate propagates through the thickness from the punch contact zone and radially outward over a cylindrical plate region of ~0.18 mm in diameter. The region 2 departure from linearity is due to continued propagation of the yield surface in the plate radially outward but over much larger portions

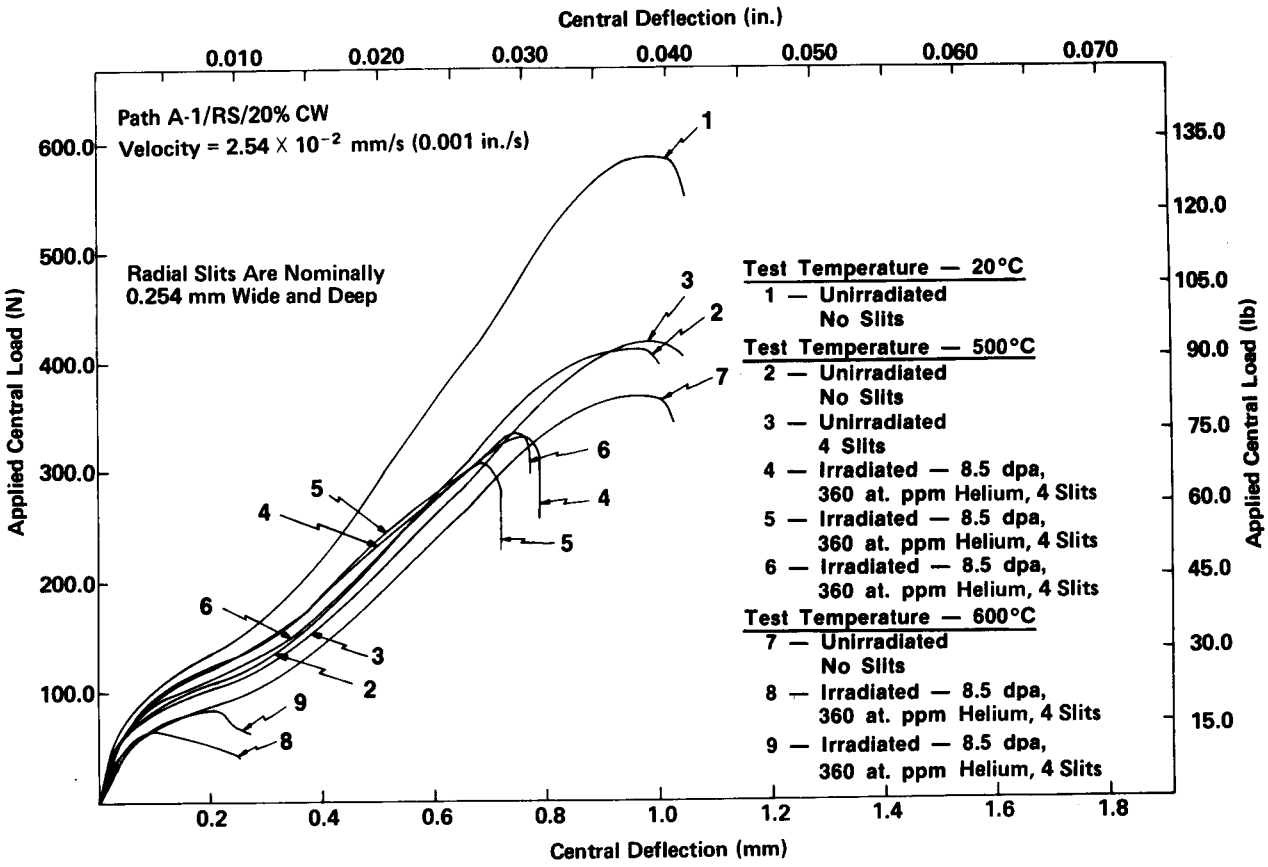

Fig. 17. Postirradiation data for Path A-1/RS/20% CW material.

of the plate. In essence, the bulk of the plate is yielding, and thus region 2 is governed primarily by the yield stress of the material.

The ratio of the outermost fiber radial stress components on the plate top and bottom surfaces for two radial locations as a function of the punch central deflection was plotted to assess the range of central deflections over which the transition from bending to membrane stressing regime occurs. The transition occurs for central deflections between ~0.18 and 0.38 mm. Thus, region 3 illustrates the portion of the central load/deflection curve where the transition from bending to membrane stressing regime occurs in most regions of the plate. In region 4, the membrane stressing regime is dominant in most regions of the plate. These stresses eventually lead to fracture in region 5 on the bottom of the plate. An investigation to determine approximately where on the central load/deflection curve fracture initiates for Types 302 and 316 stainless steel (N-LOT) was performed. The results of the fracture initiation investigation are shown in Figs. 22 and 23. For both materials, the fracture initiates prior to the load peak. Fracture has been observed to occur at a radial location of ~0.254 mm for the Type 302 stainless steel shim stock specimens. The fracture load range for the N-LOT material occurs somewhat closer to the load peak in comparison with the Type 302 stainless steel shim stock data because of the larger ductility of the N-LOT material.

The load drop in the MDBT is actually due to two causes. The first is through thickness thinning of the plate near the punch which decreases the load carrying capacity. The second is fracture with subsequent through thickness and circumferential crack propagation.

VIII. SUMMARY AND CONCLUSIONS

There are many promising advanced alloy systems for various nuclear applications. The mechanical behavior of prime candidates from each of these alloy systems needs to be readily determined in the postirradiated state. A new mechanical behavior test has been successfully developed to achieve this goal. Since neutron irradiation costs scale with specimen volume, this miniaturized mechanical behavior test can now provide significant savings in irradiation testing costs for nuclear materials investigations.

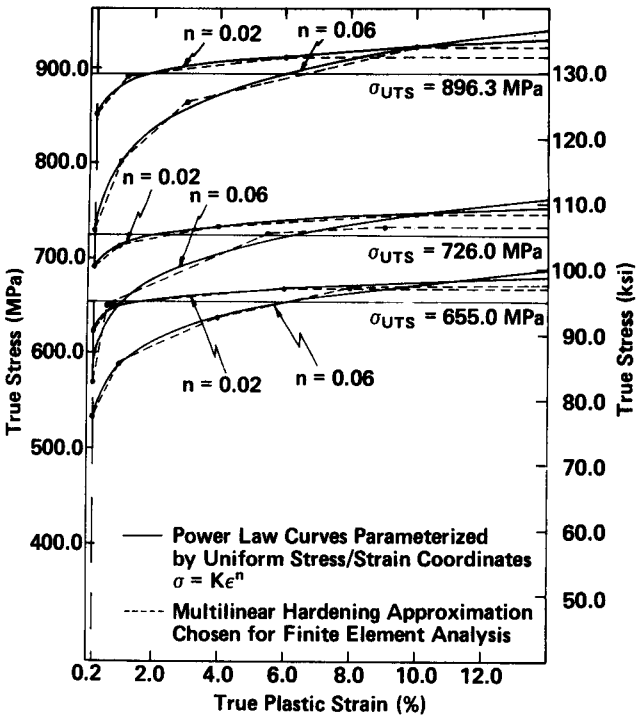

Fig. 18. Spectrum of parameterized flow curves used to invert postirradiation data.

Based on the research reported herein, the following conclusions can be stated:

1. The MDBT methodology has been successfully developed and is capable of extracting postirradiation stress/strain behavior and ductility information at elevated temperatures from biaxial stress field measurements using disk-shaped specimens no larger than those used for TEM.

2. A new friction-gap finite element boundary condition model of general applicability to a wide variety of nonlinear boundary value problems has been developed and quite adequately models the shifting frictional contacts present in the MDBT.

3. The validity of the MDBT methodology has been demonstrated using a material with well-characterized mechanical behavior.

4. A postirradiation data inversion strategy using the finite element method has been developed and successfully applied to irradiated samples to convert the MDBT applied central load/deflection curves to stress/strain behavior information.

5. The results of this work indicate that the MDBT methodology is capable of delivering uniaxial stress/strain information with approximately the

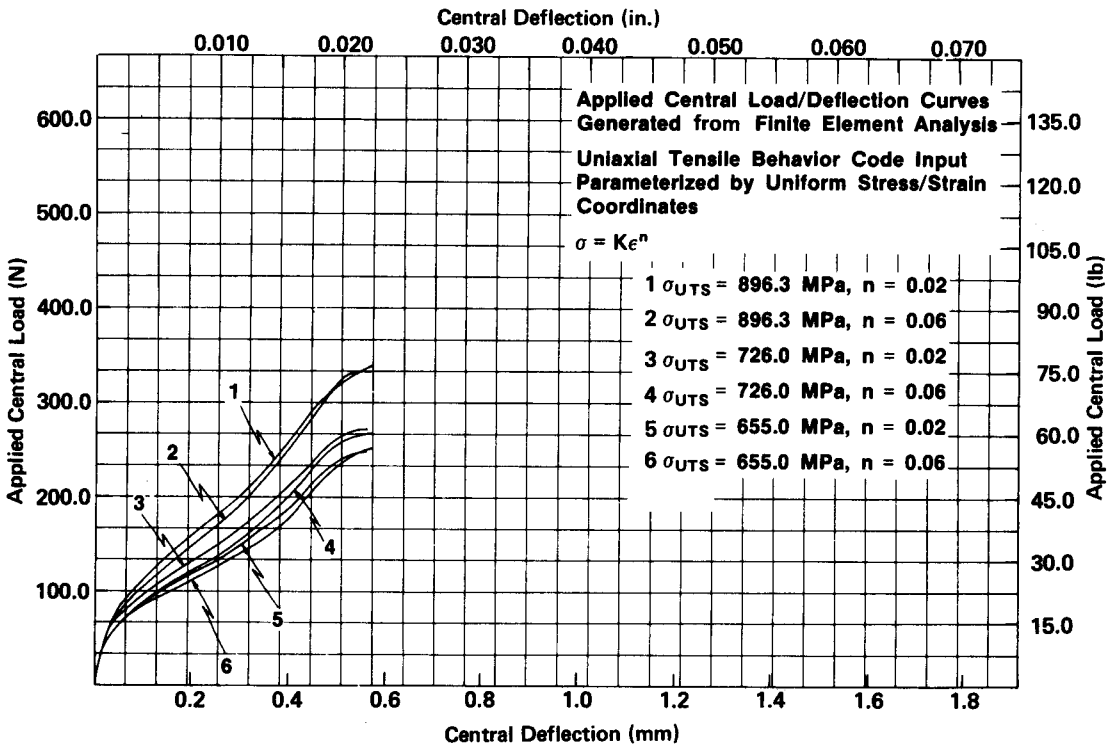

Fig. 19. Spectrum of applied central load/deflection curves generated from finite element analysis using parameterized flow curves.

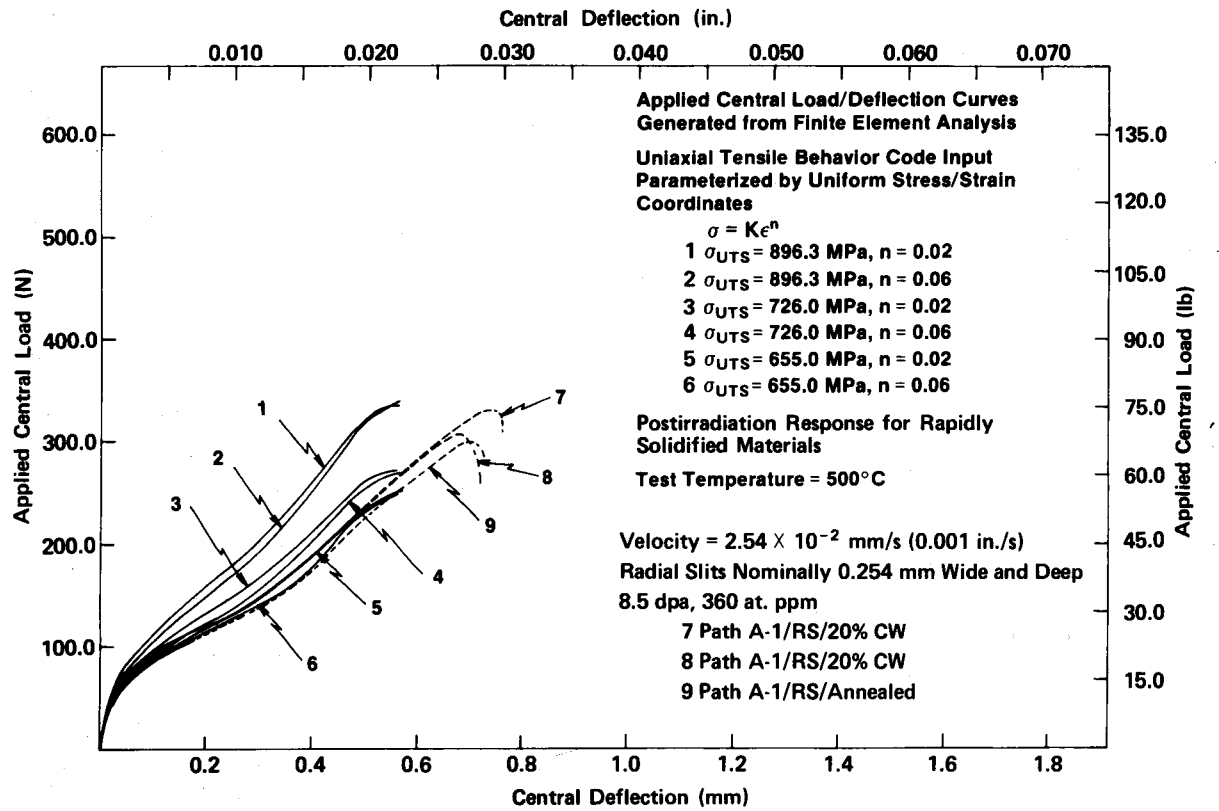

Fig. 20. Postirradiation data inversion of RS materials using MDBT methodology.

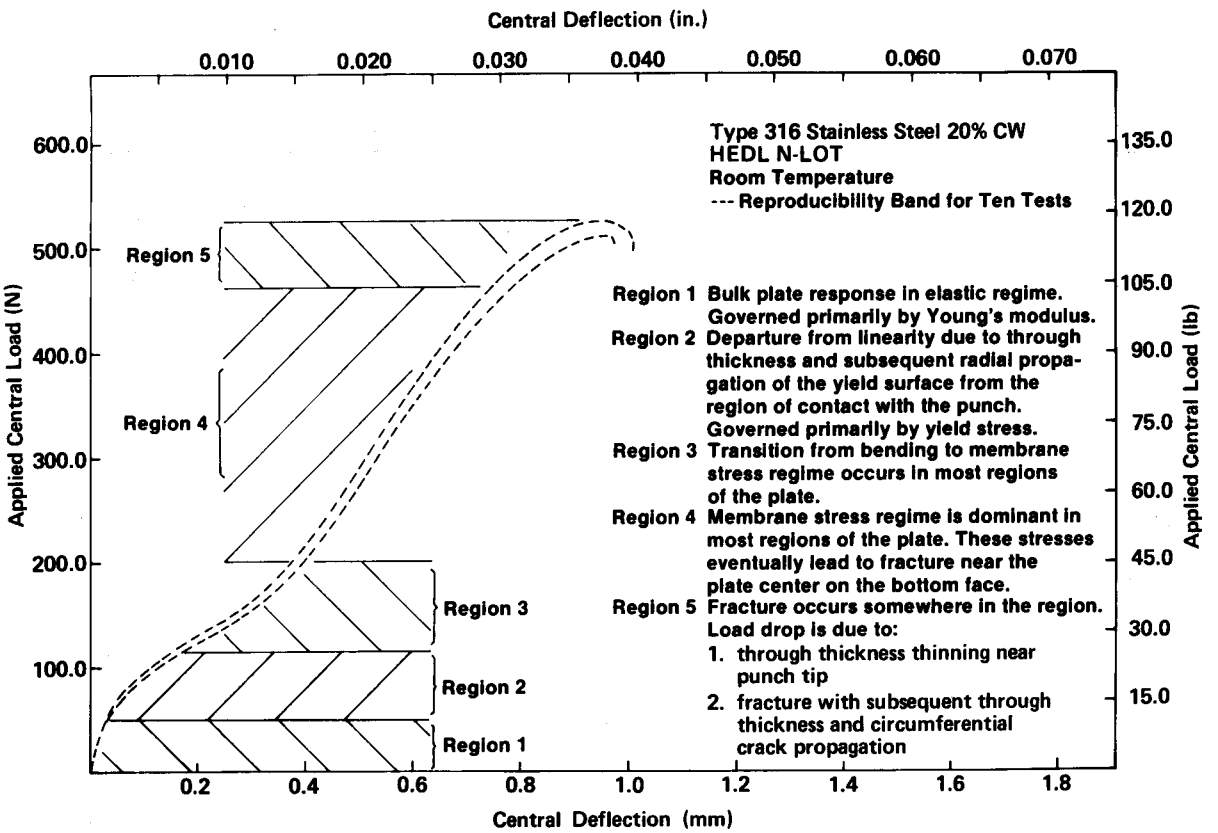

Fig. 21. Fundamental interpretation of applied central load/deflection curves for Type 316 stainless steel 20% CW.

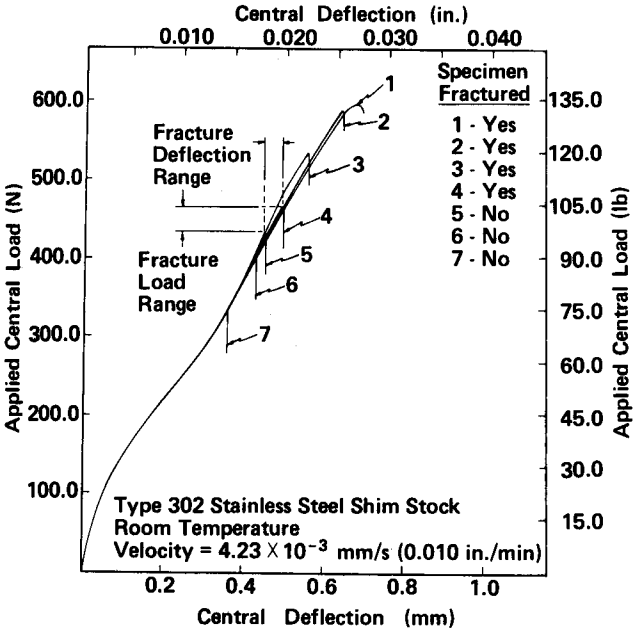

Fig. 22. Results of fracture initiation investigation for Type 302 stainless steel.

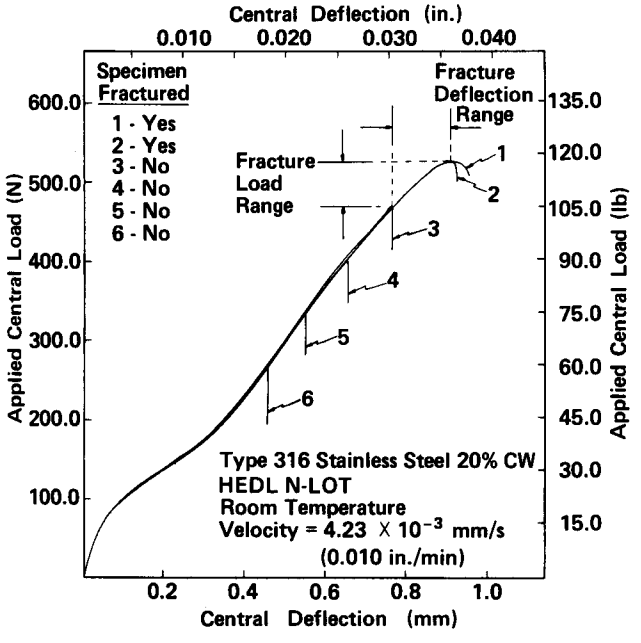

Fig. 23. Results of fracture initiation investigation for Type 316 stainless steel 20% CW.

same level of accuracy as that present in the more conventional uniaxial tensile testing approach.

6. The MDBT is capable of delivering information on fracture modes and fracture stress and strain.

ACKNOWLEDGMENT

This work was performed at the Massachusetts Institute of Technology.

REFERENCES

1. H. HERBERT, "Ueber den Zusammenhang der Biegungselastizitat des GuBeisens mit seiner Zug-und Druckelastizitat," *Mitt. u Forschungsarb, Ver. deut. Ing.*, **89**, 39 (1910).

2. W. H. CROCKER, "Obtaining a Stress/Strain Relationship from a Rotary Three-Point Bend Test with Large Plastic Displacements," submitted in partial fulfillment of the requirements for the MS degree at MIT (Aug. 1979).

3. K. A. STELSON and D. C. GOSSARD, "An Adaptive Pressbrake Control Using an Elastic-Plastic Material Model," *Proc. 1981 Conf. Joint Automatic Control*, Charlottesville, Virginia, June 17-19, 1981, Vol. 11.

4. F. H. HUANG, M. L. HAMILTON, and G. L. WIRE, "Bend Testing for Miniature Disks," *J. Nucl. Technol.*, **57**, *2*, 234 (1982).

5. "Annual Report of Alloy Development for Irradiation Performance in Fusion Reactors," by MIT Project Staff, Alloy Development Project, September 1979-September 1980, Report No. MITNRL-006 and DOE/ER-10107-1 (Dec. 1980).

6. H. YU and J. C. M. LI, "Computer Simulation of Impression Creep by the Finite Element Method," *J. Mater. Sci.*, **12**, 2214 (1977).

7. S. N. G. CHU and J. C. M. LI, "Impression Creep; A New Creep Test," *J. Mater. Sci.*, **12**, 2200 (1977).

8. S. N. G. CHU and J. C. M. LI, "Impression Fatigue," *Scripta Met.*, **13**, 1021 (1979).

9. M. P. MANAHAN, "The Development of a Miniaturized Disk Bend Test for the Determination of Post-Irradiation Mechanical Behavior," ScD Thesis, Massachusetts Institute of Technology (1982).

10. M. P. MANAHAN, A. S. ARGON, and O. K. HARLING, "The Development of a Miniaturized Disk Bend Test for the Determination of Post-Irradiation Mechanical Properties," *J. Nucl. Mater.*, **103** and **194**, 1545 (1981).

11. M. P. MANAHAN, A. S. ARGON, and O. K. HARLING, "Mechanical Behavior Evaluation Using the Miniaturized Disk Bend Test," *Sixteenth Quarterly Technical Progress Report on Damage and Fundamental Studies*, DOE/ER-0046/8, p. 82, (Oct.-Dec. 1981).

12. Standard E8, "Tension Testing of Metallic Materials," *1980 Annual Book of ASTM Standards*, Part 10, Metals-Physical, Mechanical, Corrosion Testing, American Society for Testing and Materials, p. 197 (1980).

13. M. M. PAXTON, "Mechanical Properties of Prototypic FTR Cladding—20% C.W. 316 Stainless Steel Tubing," HEDL-TME 71-59, Hanford Engineering Development Laboratory (1971).

14. J. M. STEICHEN, "High Strain Rate Tensile Properties of 20% C.W. Type 316 Stainless Steel," HEDL-TME 74-39, Hanford Engineering Development Laboratory (1974).

15. K. J. BATHE, "Automatic Dynamic Incremental Nonlinear Analysis (ADINA)," MIT 82448-1, Massachusetts Institute of Technology (1978).

16. H. D. HIBBITT, B. I. KARLSSON, and E. P. SORENSEN, "ABAQUS; A General Purpose Finite Element Code," developed by Hibbitt, Karlsson, and Sorensen, Inc., Providence, Rhode Island (1982).

17. A. NAGAMATSU, T. MUROTA, and T. JIMMA, "On the Non-Uniform Deformation of Material in Axially Symmetric Compression Caused by Friction," *Bull. J. SME*, **15**, 1339 (1972).

18. A. NAGAMATSU, T. MUROTA, and T. JIMMA, "On the Non-Uniform Deformation of a Block in Plane-Strain Compression Caused by Friction," *Bull. J. SME*, **14**, 322 (1971).

19. J. L. GORDON and A. S. WEINSTEIN, "Finite Element Analysis of the Plane Strain Drawing Problem," presented at the 2nd Conf. North American Metalwork Research, Madison, Wisconsin, p. 194 (1974).

20. K. IWATA, K. OSAKADA, and S. FUJINO, "Analysis of Hydrostatic Extrusion by the Finite Element Method," *J. Eng. Ind.*, **94**, 697 (1972).

21. E. J. ODELL, "Study of Wall Ironing by the Finite Element Technique," *J. Eng. Ind.*, **100**, 31 (1978).

22. S. N. SHAH and S. KOBAYASHI, "Rigid-Plastic Analysis of Cold Heading by the Matrix Method," *Proc. 15th Conf. Int. MTDR*, Birmingham, Alabama, 1974, p. 603, Halstead Press, division of John Wiley & Sons, Inc., New York (1975).

23. H. MATSUMOTO, S. I. OH, and S. KOBAYASHI, "Note on the Matrix Method for Rigid Plastic Analysis of Ring Compression," *Proc. Conf. 18th Int. Tool Design and Research* and *Proc. 18th Conf. Int. MTDR*, Imperial College, London, 1977, p. 3, MacMillan Press, Ltd., London (1978).

24. F. W. SHARMAN, Electricity Council Report R581 (1975).

25. O. C. ZIENKIEWICZ, P. C. JIAN, and E. ONATE, "Flow of Solids During Formation and Extrusion: Some Aspects of Numerical Solutions," *Int. J. Solids Structure*, **14**, 15 (1978).

26. P. HARTLEY, C. E. N. STURGESS, and G. W. ROWE, "Friction in Finite-Element Analyses of Metalforming Processes," *Int. J. Mech. Sci.*, **21**, 301 (1978).

27. J. J. A. ROADAL, "Finite-Element Large-Deflection Finite-Strain Elastic-Plastic Transient Response Analysis of Structures," PhD Thesis, Massachusetts Institute of Technology (1974).

28. E. RABINOWICZ, *Friction and Wear of Materials*, John Wiley & Sons, Inc., New York (1965).

29. R. L. FISH, N. S. CANNON, and G. L. WIRE, "Tensile Property Correlations for Highly Irradiated 20 Percent Cold-Worked Type 316 Stainless Steel," *Effects of Radiation on Structural Materials*, ASTM STP 683, p. 450, J. A. SPRAGUE and D. KRAMER, Eds., American Society for Testing and Materials (1979).